





RESEARCH ARTICLE

# Developmental trajectory of oligodendrocyte progenitor cells in the human brain revealed by single cell RNA sequencing

Kelly Perlman<sup>1,2</sup>  | Charles P. Couturier<sup>1</sup> | Moein Yaqubi<sup>1</sup> | Arnaud Tanti<sup>2</sup> | Qiao-Ling Cui<sup>1</sup>  | Florian Pernin<sup>1</sup> | Jo Anne Stratton<sup>1</sup> | Jiannis Ragoussis<sup>3</sup> | Luke Healy<sup>1</sup>  | Kevin Petrecca<sup>1</sup> | Roy Dudley<sup>1,4</sup> | Myriam Srouf<sup>1,4</sup> | Jeffrey A. Hall<sup>1</sup> | Timothy E. Kennedy<sup>1</sup>  | Naguib Mechawar<sup>2</sup> | Jack P. Antel<sup>1</sup>

<sup>1</sup>Department of Neurology and Neurosurgery, Montreal Neurological Institute and Hospital, McGill University, Montreal, Canada

<sup>2</sup>Department of Psychiatry, Douglas Mental Health University Institute, Montreal, Canada

<sup>3</sup>Department of Human Genetics and Bioengineering, McGill University and Genome Quebec Innovation Centre, Montreal, Canada

<sup>4</sup>Department of Pediatric Neurosurgery, Montreal Children's Hospital, Montreal, Canada

## Correspondence

Jack P. Antel, Department of Neurology and Neurosurgery, Neuroimmunology Unit, Montreal Neurological Institute, 3801 University Street, Montreal, Quebec H3A 2B4, Canada.  
Email: jack.antel@mcgill.ca

## Funding information

Genome Canada, Grant/Award Number: wst-164 (IR); International Progressive MS Alliance

## Abstract

Characterizing the developmental trajectory of oligodendrocyte progenitor cells (OPC) is of great interest given the importance of these cells in the remyelination process. However, studies of human OPC development remain limited by the availability of whole cell samples and material that encompasses a wide age range, including time of peak myelination. In this study, we apply single cell RNA sequencing to viable whole cells across the age span and link transcriptomic signatures of oligodendrocyte-lineage cells with stage-specific functional properties. Cells were isolated from surgical tissue samples of second-trimester fetal, 2-year-old pediatric, 13-year-old adolescent, and adult donors by mechanical and enzymatic digestion, followed by percoll gradient centrifugation. Gene expression was analyzed using droplet-based RNA sequencing (10X Chromium). Louvain clustering analysis identified three distinct cellular subpopulations based on 5,613 genes, comprised of an early OPC (e-OPC) group, a late OPC group (l-OPC), and a mature OL (MOL) group. Gene ontology terms enriched for e-OPCs included cell cycle and development, for l-OPCs included extracellular matrix and cell adhesion, and for MOLs included myelination and cytoskeleton. The e-OPCs were mostly confined to the premyelinating fetal group, and the l-OPCs were most highly represented in the pediatric age group, corresponding to the peak age of myelination. Cells expressing a signature characteristic of l-OPCs were identified in the adult brain in situ using RNAScope. These findings highlight the transcriptomic variability in OL-lineage cells before, during, and after peak myelination and contribute to identifying novel pathways required to achieve remyelination.

## KEYWORDS

extracellular matrix, myelination, oligodendrocytes, progenitors, single cell RNA sequencing

## 1 | INTRODUCTION

Studies of oligodendrocyte (OL) development indicate that oligodendrocyte progenitor cell (OPC) differentiation follows a complex, tightly

regulated, multistep sequence with identifiable gene expression patterns (Baldassarro et al., 2019). Unlike rodents, the rate of myelinogenesis in humans peaks in the early postnatal years (Semple, Blomgren, Gimlin, Ferriero, & Noble-Haeusslein, 2013). OPCs have

been identified in the parenchyma of normal adult CNS in humans, as well as in adult animals (Fernandez-Castaneda & Gaultier, 2016). OPCs are required for remyelination to occur in the central nervous system following exposure to OL/myelin toxins (Blakemore & Franklin, 2008). Although progenitors are present throughout life, human histologic studies and animal-based experimental studies indicate that the extent of remyelination is highly variable and age limited (Miron, Kuhlmann, & Antel, 2011). The precise molecular identity of progenitors partaking in the myelination/remyelination process in humans continues to be defined.

Single cell RNA sequencing (scRNA-seq) allows for a highly specific characterization of the transcriptomic heterogeneity of OL-lineage cells that is not achievable with microarray or bulk sequencing techniques. Murine scRNA-seq studies have advanced the characterization of OL-lineage transcriptomic signatures, with several studies identifying intermediate states between progenitors and fully differentiated cells (Artegiani et al., 2017; Marques et al., 2016; reviewed in van Bruggen, Agirre, & Castelo-Branco, 2017). Human tissue-based studies that focus on OL-lineage cells have applied sequencing of nuclei (snRNA-seq) derived from postmortem tissues from adult "control" donors and individuals with clinical conditions that include MS (Jakel et al., 2019; Schirmer et al., 2019), Alzheimer's disease (Mathys et al., 2019), and autism (Velmesshev et al., 2019). However, studies of human OL-lineage development remain limited by the availability of whole cell samples that would permit inclusion of non-nuclear RNAs, and material that encompasses a wide age span including time of peak myelination. Additionally, postmortem studies face the technical challenge that the integrity of the RNA is compromised when compared to surgical tissue studies.

In the current study, we applied single whole cell RNA sequencing to immediately ex vivo OL-lineage cells derived from surgically resected fetal, pediatric, adolescent, and adult brain specimens. The use of surgical material allowed us to recover viable cells from which whole cell scRNA-seq could then be performed. Critically, the pediatric samples coincide with a time of peak myelination ongoing in the human brain. The inclusion of tissue from such a wide age range allowed us to construct a more complete developmental trajectory of human OLs and establish transcriptomic signatures for each emergent subpopulation.

## 2 | MATERIALS AND METHODS

### 2.1 | Surgical samples

Pediatric, adolescent, and adult tissue samples resected during surgical procedures were processed for cell isolation within 1–2 hours. Summarized in Supporting Information Table S1, samples used in the current study were derived from two 2-year olds with hemimegalencephaly and Rasmussen's encephalitis respectively, a 13-year-old with intractable nonmalignant epilepsy, and two adults (58 and 62-year olds) with a subcortical glioma and nontumor related epilepsy (hippocampal sclerosis) respectively. The samples were comprised

predominantly but not exclusively of white matter and selected to exclude, as well as possible, the focal and/or diffuse pathologic substrates of these cases based on inspection during the operative procedure and retrospective histologic analyses. Surgical samples were collected by CUSA bag sample separately from subsequent dissection of pathologic tissue site. Use of pediatric, adolescent, and adult tissues was approved by the Montreal Neurological Institute and Hospital (MNI/H) Neurosciences Research Ethics Board; use of pediatric and adolescent samples were approved by the Montreal Children's Hospital Research Ethics Board. Second-trimester fetal telencephalon human brain samples were collected during elective abortions, acquired from the University of Washington Birth Defects Research Laboratory. Single cells were obtained following mechanical and enzymatic (trypsin) dissociation as previously described (Cui et al., 2017) and an isotonic percoll gradient was used to remove myelin. The whole dissociated cell population was collected from the gradient (which sits between the myelin layer and the red blood cell layer), washed 3 times in PBS, and re-suspended at a concentration of  $10^6$  cells per ml. Next, 100,000–200,000 cells were submitted for sequencing at Génome Québec. Library preparation was performed as previously described (Couturier et al., 2018). Integrity of isolated cells was further determined by establishing these cells in dissociated cell culture.

### 2.2 | Sequencing and preprocessing

ScRNA-seq libraries were created using 10X Chromium v2.0 and sequenced with the Illumina HiSeq4000 PE75 at the McGill University and Génome Québec Innovation Centre. ScRNA-seq was performed using a droplet sequencing approach (10X Chromium). All data demultiplexing and genome mapping was done using the Cell Ranger analysis pipeline (<https://github.com/10XGenomics/cellranger>). Reads were aligned to reference genome GRCh38. Multiple runs were aggregated and normalized to the same sequencing depth.

Preprocessing was done using a standard signal processing pipeline as described by Couturier et al. (2018), which removes artifacts, normalizes gene expression levels, selects genes carrying the relevant signal and increases signal-to-noise ratios. Briefly, cells found to express more than 12% mitochondrial genes were removed from analysis to eliminate any dying or dead cells (Ilicic et al., 2016). Cells were excluded if they were found to express fewer than 1,000 genes. Moreover, any cells with fewer than 1,800–2,000 unique molecular identifiers (UMI) were removed, with the minimum being dependent on the specific sample. Genes with a zero count (i.e., genes that were not detected in the sample) were automatically removed and UMI counts were normalized for each cell. Principal component analysis (PCA) was used to reduce the high-dimensionality datasets to a lower dimensional space for visualization and to remove noise. Cell cycle scores were calculated by summing the expression of all cell cycle genes detected in each cell, which were then z-scored across all cells. Cell cycle scores  $\leq 0$  were considered to be noncycling. The principal component axes that were computed based on the noncycling cells were then projected onto the complete dataset.

## 2.3 | Data analysis

The Louvain clustering algorithm (Blondel, Guillaume, Lambiotte, & Lefebvre, 2008), a heuristic, two-step, iterative clustering algorithm, was first applied to each individual dataset, and the OL-lineage cells from each dataset were extracted and merged together. The identity of OL-lineage cells was validated using the relative expression of canonical gene markers such as PDGFR $\alpha$  for OPCs, and MBP, MOG, MAG, PLP1, and CNP for mature OLs (MOLs). Louvain clustering was then applied to the pooled, z-scored OL-lineage cells across all samples. The algorithm was set to a resolution parameter gamma of 1.

We used diffusion pseudotime (DPT) created by Haghverdi, Büttner, Wolf, Büttner, and Theis (2016) to track the patterns of expression of specific genes of interest, as identified by our differential expression analyses, over the developmental period. To quantify how genes were differentially expressed across groups, population distributions for each gene were compared using the Mann-Whitney U test and adjusted for the false discovery rate (FDR). Genes were considered to be significantly differentially expressed between groups if they had an FDR-corrected *p*-value < 0.05 and a standard absolute fold change  $\geq 2$ , which translates to an absolute  $\log_2$  FC (LFC)  $\geq 1$ . For the age-specific comparisons, any genes that were significantly differentially expressed between datasets within the same age group (*n* = 10 for pediatric, *n* = 7 for adult) were excluded to eliminate as much inter-subject variability as possible.

Significantly upregulated genes from each subpopulation were inputted to the STRING database (<https://string-db.org/>) which yielded putative protein-protein interactions coded for by the top genes from each cluster. The minimum required interaction score was set to 0.7 (high confidence). These interactions were clustered using the MCL clustering algorithm with an inflation parameter equal to 3. The gene ontology (GO) feature in StringDB was utilized to generate a list of upregulated GO biological processes. Among the significantly enriched GO terms, we curated the most biologically relevant and informative subset.

## 2.4 | Gene regulatory network construction and protein-protein interactions

To construct a gene regulatory network (GRN), data of transcription factor (TF) binding sites were obtained from the ChIP Enrichment analysis (ChEA) database (Lachmann et al., 2010). We matched our gene list with the entries of this database and retrieved TFs with FDR-corrected *p*-value < 0.05 and |LFC| > 1. Using Cytoscape software, data for TF-binding and gene expression were combined to construct a gene regulatory network. The most central genes were identified using the CentiScaPe plug-in of the Cytoscape software on the constructed GRN. To identify the complete list of TFs present in our study, we referenced the list of TFs provided by Lambert et al. (2018). Networks were formed with significant TFs in the network as well as with non-TFs with FDR-corrected *p*-value < 0.05 and |LFC| > 2 (in order to limit the number of connections).

## 2.5 | Fluorescent in situ hybridization

In situ hybridization using Advanced Cell Diagnostics RNAscope<sup>®</sup> probes and reagents was performed on stored 10  $\mu$ m frozen sections prepared from blocks of human postmortem ventromedial prefrontal cortex and mounted on Superfrost charged slides. Tissue samples were derived from adults (ages 39 and 61) without known neurologic disorders who died suddenly without prolonged agonal period. Sections were first fixed in cold 10% neutral buffered formalin for 15 min at 4°C, dehydrated by 2 min long successive ethanol baths of increasing concentration (70, 95, and 100%) and air dried for 5 min. Endogenous peroxidase activity was quenched with hydrogen peroxide reagent for 10 min, followed by protease digestion for 30 min at room temperature. The following probes were then hybridized for 2 hr at 40°C in a humidity-controlled oven (HybEZ II, ACDbio): Hs-VCAN (cat. no. 430071-C2), Hs-TNR (cat. no. 525811) and PDGFR $\alpha$  (cat. no. 604481-C3) to quantify VCAN and TNR expression in I-OPCs (PDGFRA+). Successive addition of amplifiers was performed using the proprietary AMP reagents, and the signal visualized through probe-specific HRP-based detection by tyramide signal amplification with Opal dyes (Opal 520, Opal 570 or Opal 690; Perkin Elmer) diluted 1:300. Slides were then coverslipped with Vectashield mounting medium with DAPI for nuclear staining (Vector Laboratories) and kept at 4°C until imaging. Image acquisition was performed on an Olympus FV1200 laser scanning confocal microscope. Images were taken using a 40X objective (NA = 0.95) and 60X (NA = 1.42). Images were processed with ImageJ (Rueden et al., 2017).

## 3 | RESULTS

### 3.1 | Characterization of total cell isolates

As shown in Table 1, OL-lineage cells accounted for the majority of the cells in the postnatal samples. Microglia accounted for approximately 20-40%. The remainder was composed of lymphocytes (CCL5+, CD4E+), astrocytes (GFAP+, AQP4+; <1%), and doublets, a common artifact of scRNA-seq data, which is caused by simultaneous capture of two cells in one droplet. OL-lineage cells were rare in the fetal samples, amounting to only ~1.6% of all detected cells (Table 1). An example of viable OL-lineage cells derived from the pediatric surgical samples is provided in Supporting Information Figure S1. These dissociated OL cultures were derived from aliquots of the initial cell isolation using a previously described protocol (Esmonde-White et al., 2019).

### 3.2 | Gene expression differences between OL-lineage cell subpopulations

Cluster analysis of the pooled and normalized OL-lineage cells across the age span identified three distinct subpopulations based on 5,613 genes. This gene list was generated by taking the union of the

preprocessed gene sets from each age group. The subpopulations identified were comprised of an early progenitor group (e-OPC), a late progenitor group (l-OPC), and an MOL group (Figure 1a). A cell-cell correlation map illustrating the clustering graphically is presented in Supporting Information Figure S2.

Based on our significance criteria, differential expression analysis between the three subpopulations shows that in the e-OPC group, 500 genes (8.9%) were upregulated and 103 genes (1.8%) were downregulated compared to the l-OPCs and the MOLs. In the l-OPC group, 338 genes (6%) were upregulated and 75 genes (1.3%) downregulated compared to the e-OPCs and MOLs. In the MOL group, 94 genes (1.7%) were upregulated and 370 genes (6.6%) downregulated

compared to the e-OPCs and l-OPCs. Full differential expression analysis results are presented in Supporting Information Dataset S1. Figure 1b presents pie charts with the relative percentage of upregulated vs downregulated genes for each group. Figure 1c displays a heatmap showing the differentially expressed genes between groups.

Figure 2a shows violin plots for the top five genes from each subpopulation, as determined by highest LFC (e-OPC: NNAT, IGFBP2, TMSB15A, SOX11, FABP7; l-OPC: TNFR, VCAN, PTPRZ1, FERMT1, NEU4; MOL: CRYAB, PPP1R14A, PLP1, MBP, PTGDS) and provides a visual comparison of the expression of these genes in the other two cell subpopulations. Of note, genes specific to myelination were found to

**TABLE 1** Properties of cell yield from scRNA-seq organized by age group

Age range	Group	n	Total cell count	OL-lineage cell count	% OL-lineage in total count
Second trimester	Fetal	4	22,637	359	1.59
2 years	Pediatric	2	5,893	3,432	58.24
13 years	Adolescent	1	4,037	3,086	76.44
58 and 62 years	Adult	2	5,418	3,510	64.78
Total		9	37,985	10,387	27.35

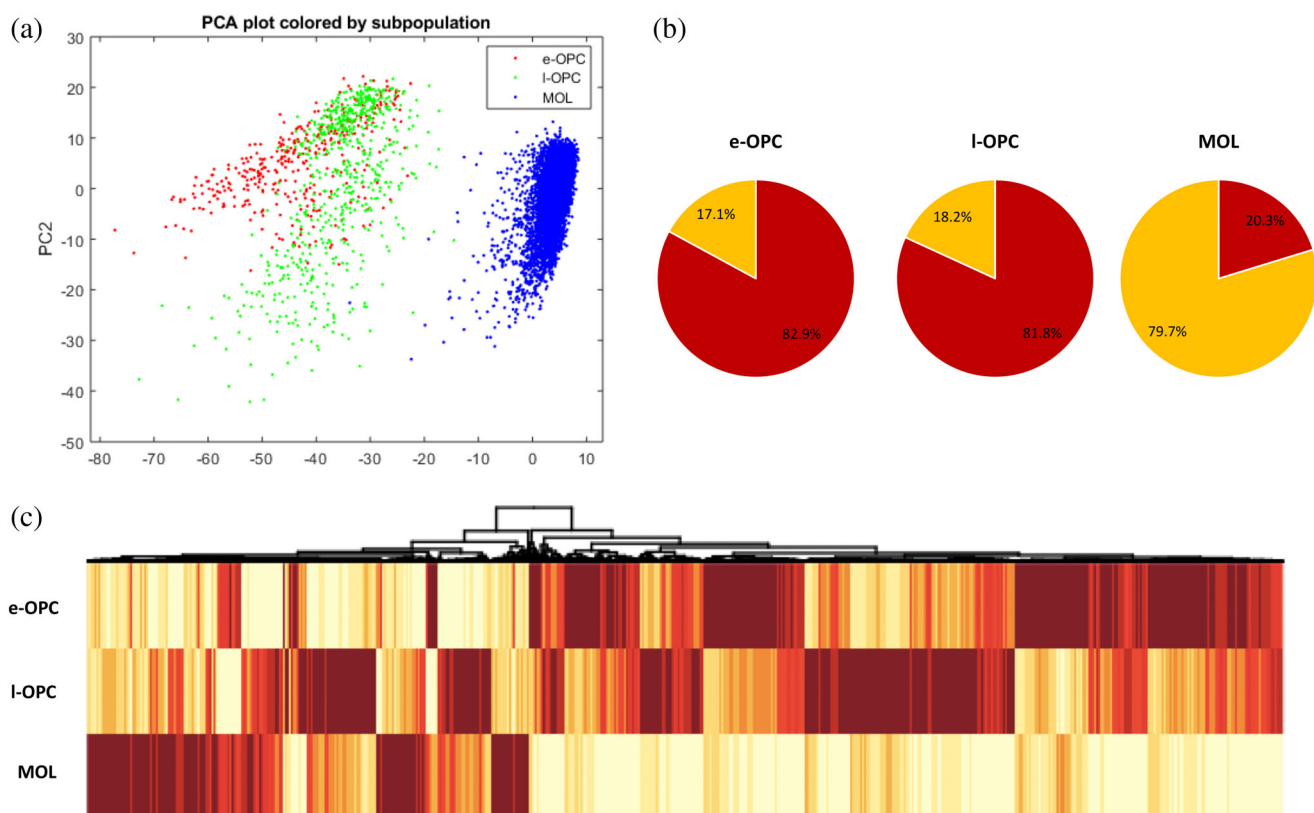


**FIGURE 1** (a) PCA plots of pooled sample colored by OL-subpopulation as determined by unbiased clustering algorithm. Red = early OPCs (e-OPC); Green = late OPCs (l-OPC); Blue = mature oligodendrocytes (MOL). (b) Pie charts presenting the relative percentage of upregulated (red) and downregulated (yellow) genes for each subpopulation. (c) Heat map with corresponding dendrogram showing e-OPC, l-OPC, and MOL gene expression relative to each other. Darker colors represent higher expression levels [Color figure can be viewed at [wileyonlinelibrary.com](http://wileyonlinelibrary.com)]

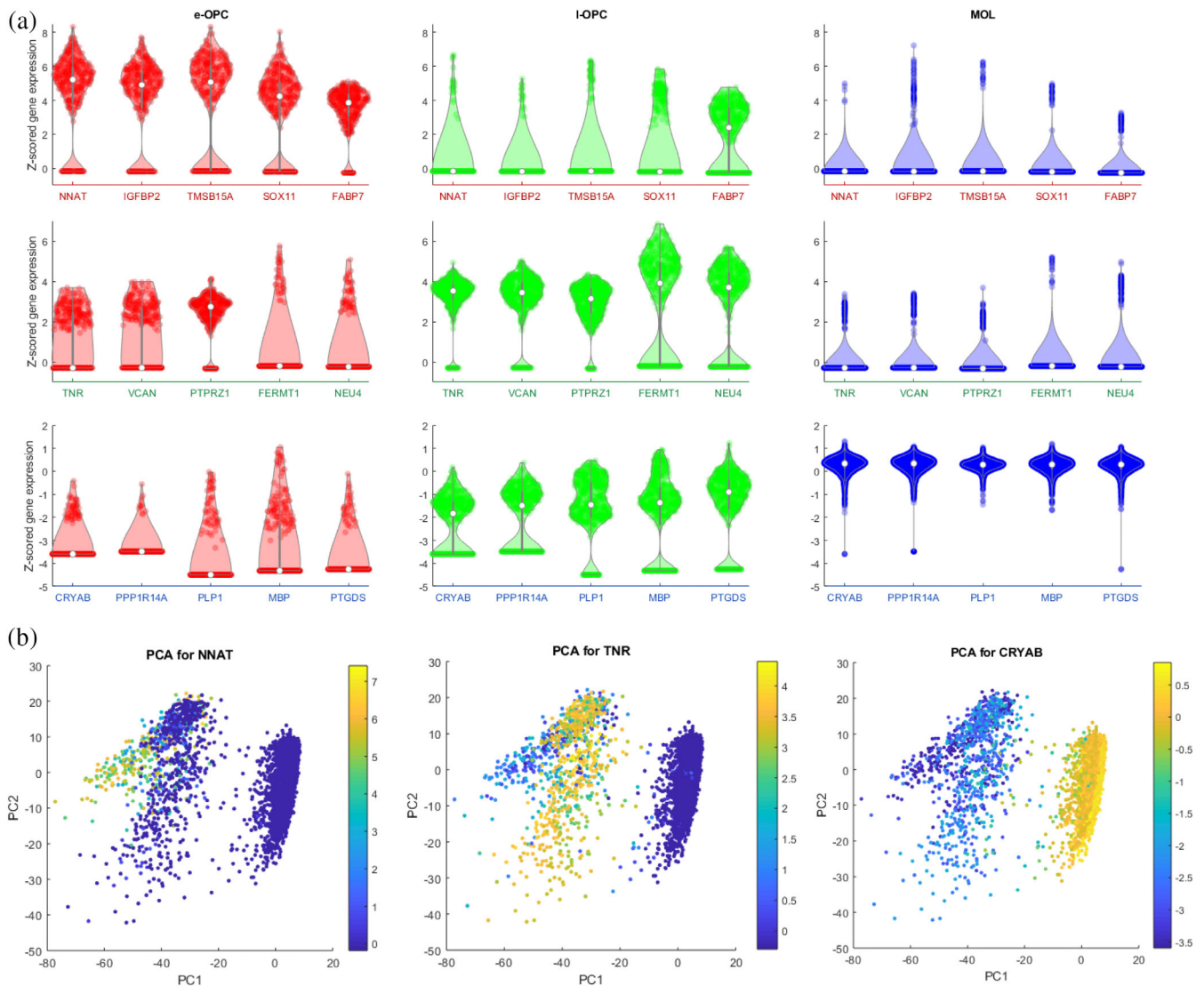


**FIGURE 2** (a) Violin plots comparing the expression of the top from five genes from each OL-lineage subpopulation as defined by top log fold change. (b) Representation of the expression of the top gene from each subpopulation as defined by log fold change on PCA plots, with each top gene showing high specificity to its respective cluster. Color bar represents expression on a z-scored log base 2 scale [Color figure can be viewed at [wileyonlinelibrary.com](http://wileyonlinelibrary.com)]

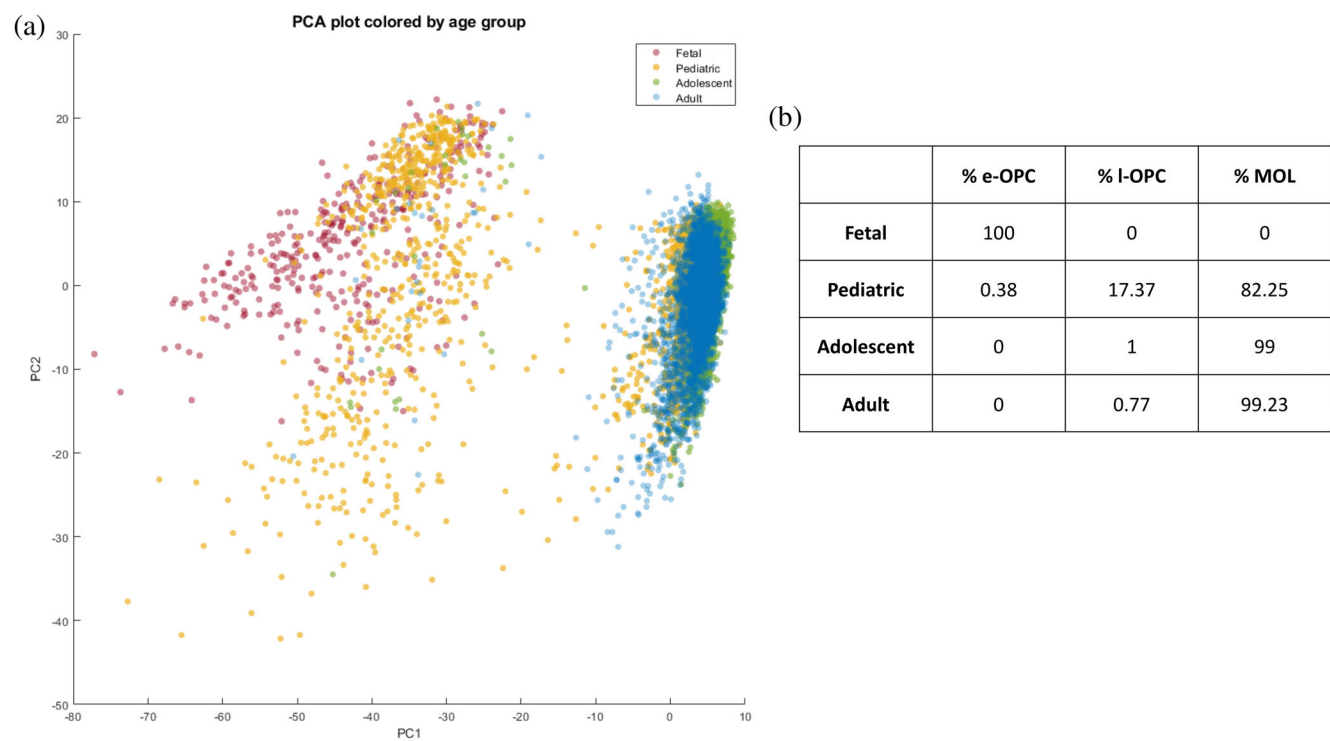
be expressed by the I-OPC population at a level intermediate to the expression levels found for e-OPC and MOL, suggesting graded rather than binary regulation of expression. Projecting the expression of the top gene from each subpopulation onto PCA plots (Figure 2b) illustrates that each top gene shows high specificity to its respective cluster.

Figure 3a demonstrates age-specific differences in subpopulation distribution graphically on a PCA plot, with points colored by age. Figure 3b indicates the distribution of the three OL-lineage subpopulations in relation to donor age group; the frequency of cells at a given age is expressed by the percentage of total OL-lineage cell count. Notably, the relative distribution of the adolescent and adult OL-lineage cells is almost identical.

To avoid biasing the DPT trajectory a result of the differing sizes of the subpopulations, the number of cells in I-OPCs and MOLs was down sampled to match the number of cells in e-OPCs, thus allowing

for each subpopulation to have an equal representation across pseudotime. The expression of the top five differentially expressed genes from each subpopulation plotted across the stages of differentiation revealed subpopulation-specific patterns of gene expression (Figure 4a). As shown, the top e-OPC genes peak at the earliest pseudotime point, top I-OPC genes peak slightly later, and top MOL genes peak much later. The expression of canonical lineage markers (PDGFR $\alpha$ , CSPG4/NG2, OLIG2, SOX10, PLP1, CNP, MBP, PTGDS) was then plotted across pseudotime to assess whether these patterns matched prediction from previous literature (Miller, 2002; Figure 4b). Our results show that each gene followed the overall expected patterns but also revealed more nuanced expression dynamics. For example, though PDGFR $\alpha$  and CSPG4/NG2 are both progenitor markers, CSPG4/NG2 expression peaks in pseudotime later than PDGFR $\alpha$  expression.





**FIGURE 3** Distribution of OL-lineage subpopulations within each age group. (a) Graphical representation of the age-specific differences in subpopulation distribution on a PCA plot, with points colored by age. (b) Distribution of OL-lineage subpopulations within each age group. The frequency of cells in a given subpopulation for a given age is expressed by % of total OL-lineage cell count [Color figure can be viewed at [wileyonlinelibrary.com](#)]

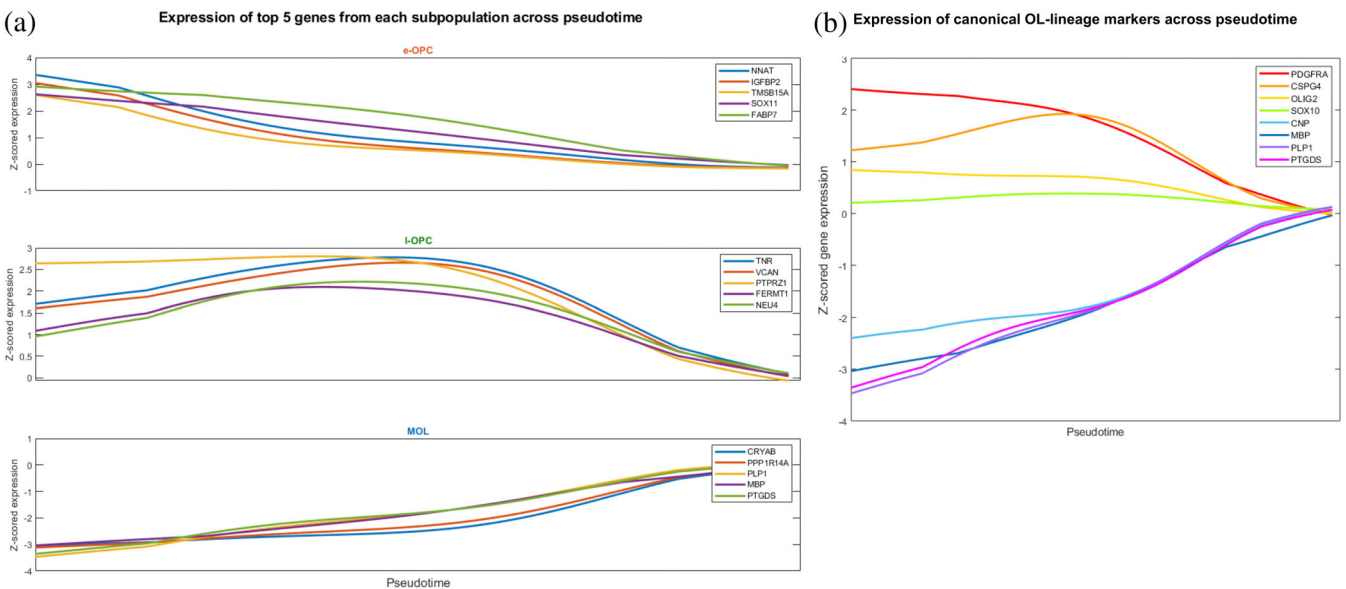


**FIGURE 4** (a) Expression of top five genes from each subpopulation tracked across pseudotime to reveal population-specific expression patterns. (b) Expression of canonical OL-lineage genes tracked across pseudotime to assess that their expression matches the expected patterns [Color figure can be viewed at [wileyonlinelibrary.com](#)]

### 3.3 | Biological pathways linked to distinct OL-lineage cell subsets

To investigate potential functional correlates of the subpopulation specific patterns of gene expression, GO analysis was conducted with the

significantly upregulated genes from each subpopulation, which identified respective top upregulated biological pathways (Figure 5a). For MOLs, upregulated pathways identified include myelination, regulation of transport, organelle organization and intracellular iron sequestration when compared to both e-OPCs and I-OPCs. Since several pathways were common

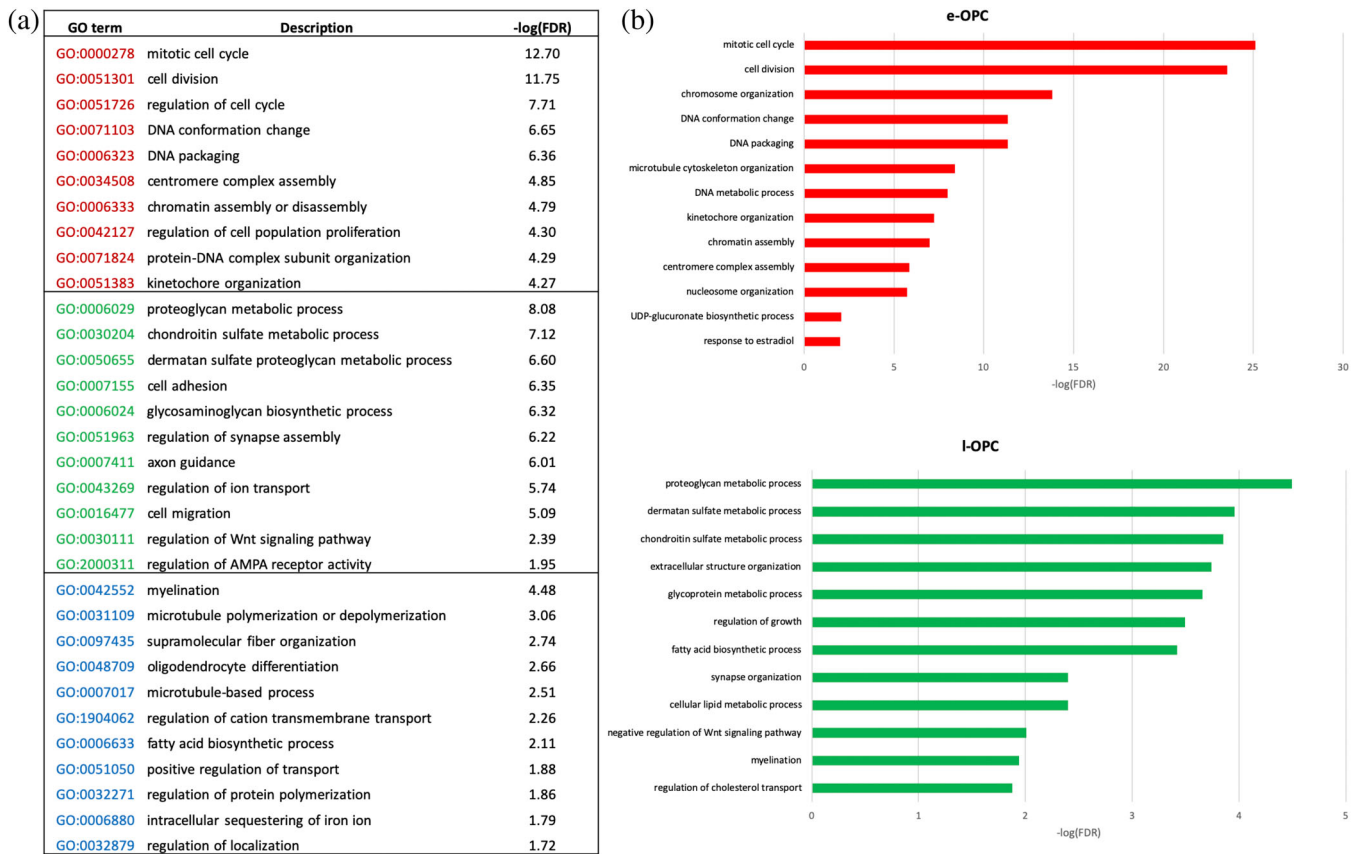


**FIGURE 5** (a) Top biological pathways enriched each OL-lineage subpopulation as determined by gene ontology. (b) Top biological pathways enriched in e-OPC and I-OPC derived from two-way differentially expressed genes as determined by gene ontology [Color figure can be viewed at [wileyonlinelibrary.com](http://wileyonlinelibrary.com)]

between the e-OPCs and I-OPCs and to obtain a more sensitive comparison between these progenitor populations, a separate GO analysis was conducted with upregulated genes from the differential expression analysis comparing e-OPCs and I-OPCs only (FDR-corrected  $p$ -value  $< 0.05$ ,  $|\text{LFC}| > 1$ ). In e-OPCs, upregulated biological processes included regulation of the cell cycle, microtubule cytoskeletal organization, and chromatin conformation; For I-OPCs, upregulated pathways included extracellular matrix (ECM) metabolism, lipid metabolism, and myelination. (Figure 5b). StringDB-generated networks displaying the predicted protein-protein interactions within the upregulated genes from each subpopulation can be found in Supporting Information Figures S2–S4 and provide information on the sub-clusters of co-expressed genes. For example, the I-OPC contains modules of genes coding for the ECM and collagens, axon guidance molecules, ionotropic glutamate receptors, g-coupled protein receptors, and synaptic proteins. These modules are interlinked with each other via highly interconnected nodes that include the genes GPR17, GRM5, NTN1, FYN, TRIO, SDC3, GRIA2, and GRIA3 (Supporting Information Figure S4).

### 3.4 | Transcription factors associated with the OL-lineage cell subset

Transcription factors drive changes in gene expression, and often find utility as markers of cellular differentiation. To identify differential

expression of transcription factors in the subpopulations identified in the current study, the gene expression data was filtered based on a list of human transcription factors reported by Lambert et al. (2018). Fifty transcription factors were identified that are differentially expressed in at least one subpopulation (Figure 6a). TFs that were selectively expressed in one subpopulation as compared to the other two include: MYC, ZNG385D, MYT1L, DLX1, HES4, FOXM1 in e-OPCs; HMGA1, PRRX1, E2F3, SOX21, HIF3A, ZNF469, and SOX8 in I-OPCs; and CREB5, MYRF, JUND in MOLs. Centrality analysis indicated that SOX2 was the most highly connected TF in e-OPC, I-OPC, and MOL (Figure 6b–d), consistent with its key role in regulating the OL lineage (Liu et al., 2013).

### 3.5 | Age-specific subpopulation comparisons

We directly compared the I-OPC and MOL populations for the pediatric and adult donors. The MOL populations between age groups were remarkably similar, with only two genes being significantly (FDR-corrected  $p$ -value  $< 0.05$ ,  $|\text{LFC}| > 1$ ) differentially expressed (LINC00844 and CLU upregulated in adult MOLs). On the other hand, the expression profiles of I-OPCs between pediatric and adult populations were quite distinct with 60 genes significantly upregulated in pediatric I-OPCs and 244 significantly upregulated in

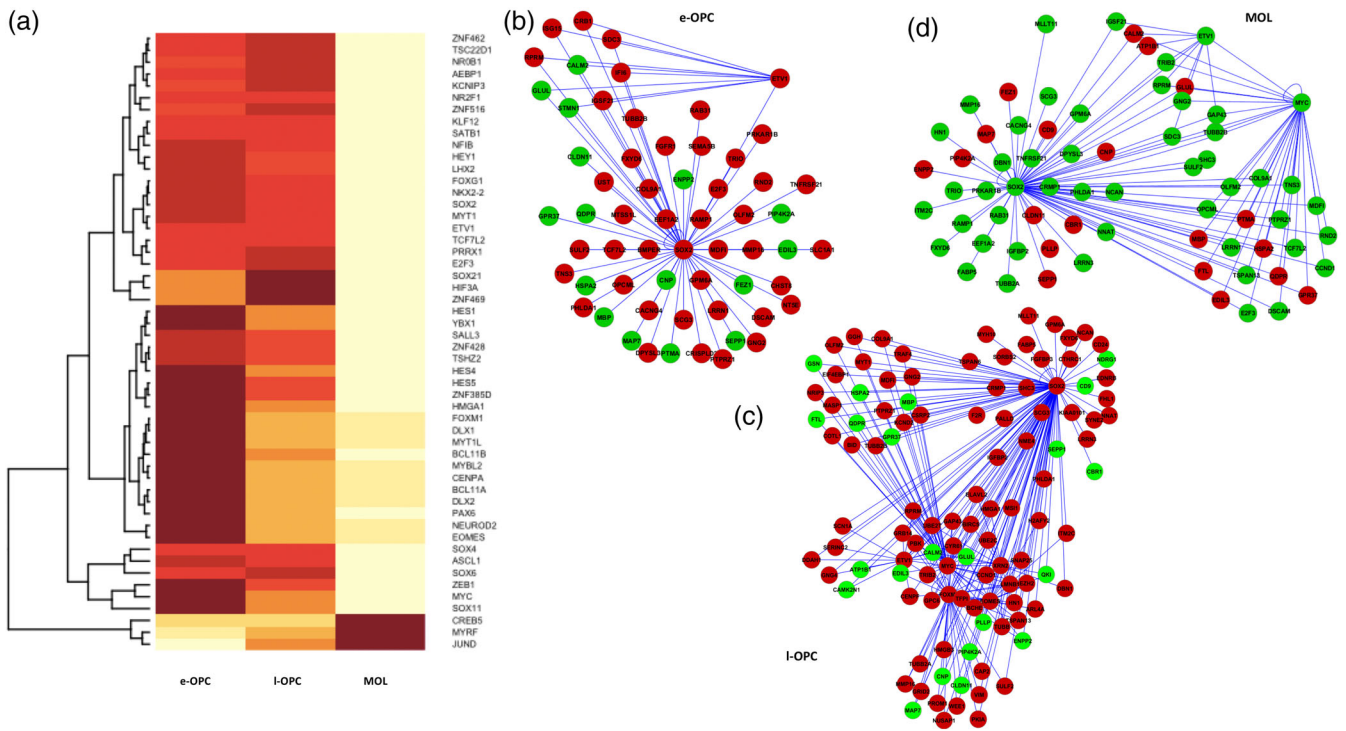


**FIGURE 6** (a) Heatmap comparing expression of transcription factors across subpopulations. SOX2 hub gene networks for (b) e-OPCs, (c) I-OPC, and (d) MOLs. Red nodes = upregulated gene, green node = downregulated gene [Color figure can be viewed at [wileyonlinelibrary.com](#)]

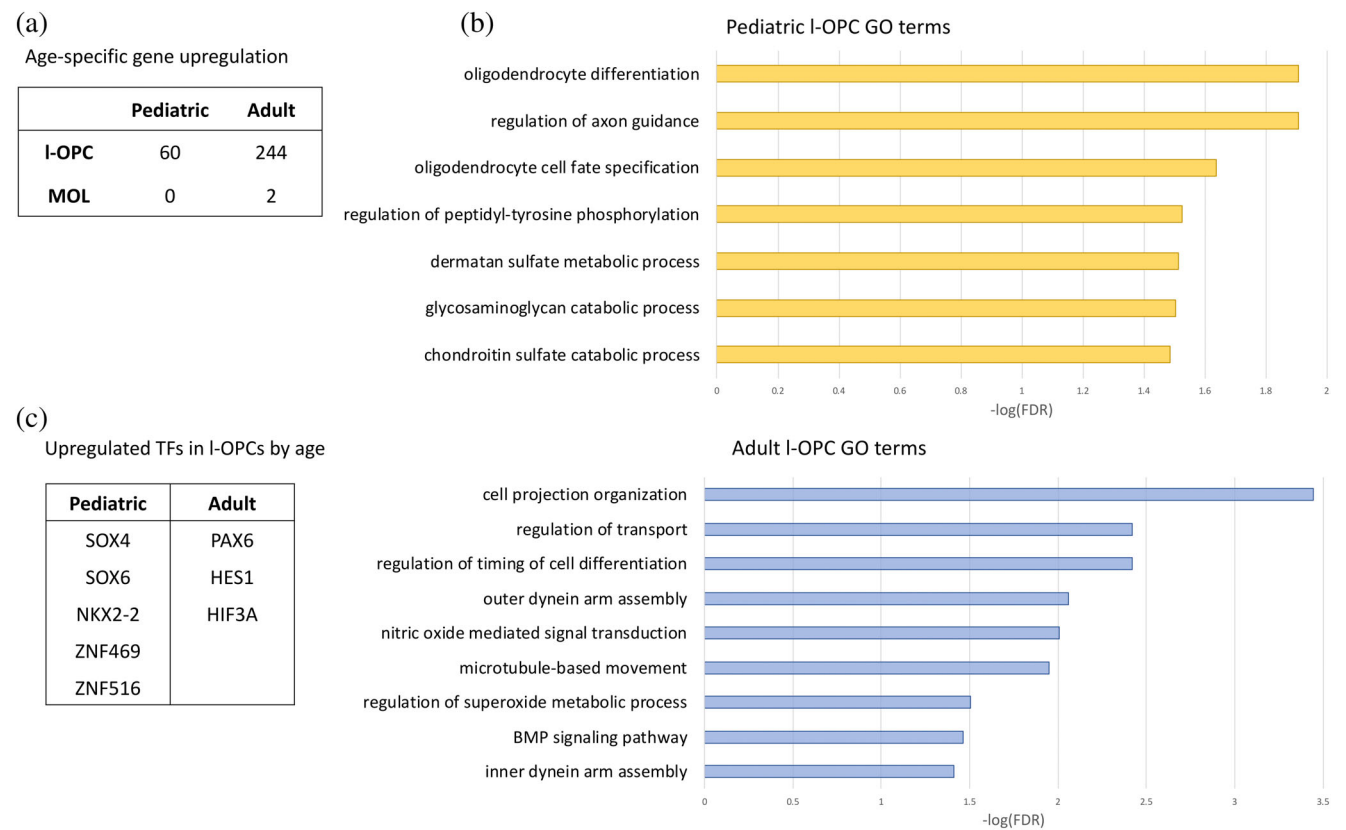


**FIGURE 7** (a) Number of significantly upregulated genes in pediatric and adult cells for I-OPCs and MOLs. (b) Top biological pathways enriched in pediatric I-OPCs and adult I-OPCs, as determined by gene ontology, based on their respective significantly upregulated genes. (c) Significantly upregulated transcription factors specific to pediatric and adult I-OPCs [Color figure can be viewed at [wileyonlinelibrary.com](#)]



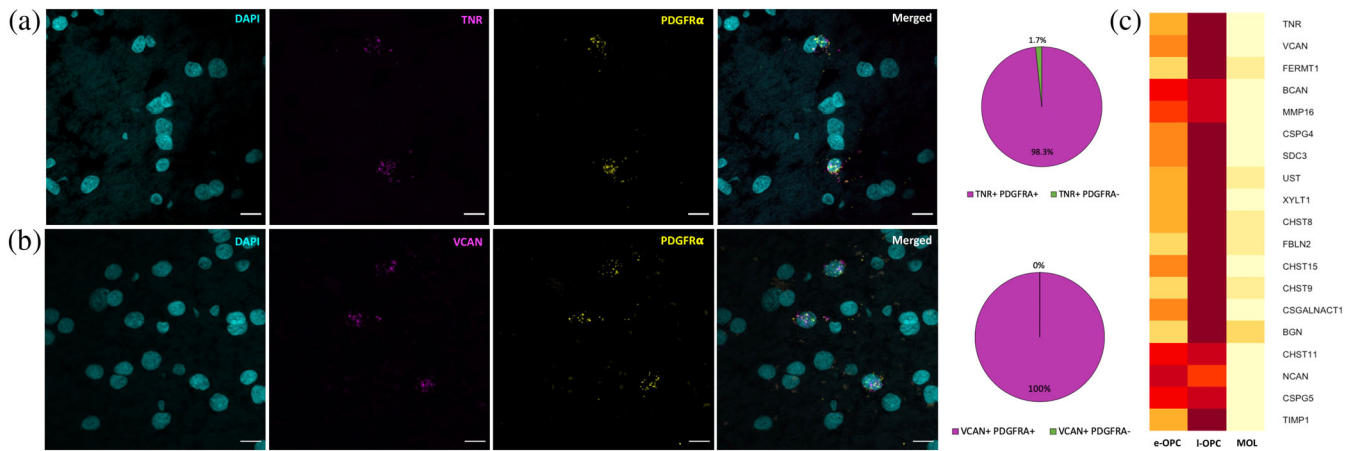


**FIGURE 8** Enrichment of extracellular matrix gene expression in late OPCs was validated using single molecule fluorescent in situ hybridization (RNAscope). Representative confocal images of I-OPCs identified based on PDGFRα expression (yellow) and showing co-expression with (a) TNR and (b) VCAN (magenta). Pie charts illustrate that 98.3% of TNR-expressing cells are I-OPCs ( $N = 60$  cells), while 100% of VCAN-expressing cells are I-OPCs ( $N = 60$  cells), indicating a strong enrichment of those genes in I-OPCs. Scale bar = 10  $\mu$ m. (c) Heatmap illustrating the z-scored expression of key extracellular matrix genes in each OL-lineage subpopulation. Genes are ordered in decreasing LFC for I-OPC [Color figure can be viewed at [wileyonlinelibrary.com](http://wileyonlinelibrary.com)]

adult I-OPCs (Figure 7a). Significantly enriched GO terms were curated from the lists generated by these upregulated genes (Figure 7b). In pediatric I-OPCs, the associated GO terms included OL differentiation, axon guidance, and metabolism of ECM components, and in adult I-OPCs, the GO terms were related to regulation of cell projections, dynein arm assembly, and superoxide metabolism. Protein-protein interaction networks for top pediatric I-OPC genes (Supporting Information Figure S6) and top adult I-OPC genes (Supporting Information Figure S7) display the relationships between the genes within each age-specific signature. Notably, MBP and CNP genes, both characteristic of myelination, were upregulated in the pediatric I-OPCs compared to the adult I-OPCs. Supporting Information Table S2 lists the top 20 genes specifically upregulated in pediatric I-OPCs and the top 20 genes specifically upregulated in adult I-OPCs, with the predicted cellular localization of their protein products. Genes encoding transcription factors that were significantly upregulated in I-OPCs in pediatric and adults are listed in Figure 7c. Full differential expression analysis results are presented in Supporting Information Dataset S2.

### 3.6 | In situ validation

To assess whether any cells with the signature of the relatively abundant I-OPCs present at ages associated with peak myelination could be detected in situ in the adult brain, we used RNAscope fluorescent in situ hybridization. Given that no e-OPCs were identified in our adult samples, we considered all PDGFRα+ cells to be I-OPCs. In Figure 8, PDGFRα+ cells were found to express (a) TNR and (b) VCAN in sections of adult postmortem ventromedial prefrontal cortex (98.3% TNR+/PDGFRα+; 100% VCAN+/PDGFRα+). This expression pattern was highly specific to OPCs, as these genes were not detected

in PDGFRα- cells, thus providing validation of our I-OPC signature. Many of the significantly upregulated genes in the I-OPCs are central to ECM-related biological processes (Figure 8c), with TNR and VCAN being the two top genes as determined by highest LFC.

## 4 | DISCUSSION

The current study presents human scRNA-seq OL-lineage data derived directly from immediately ex vivo cells isolated from surgically derived brain specimens covering a wide spectrum of ages. The contribution of the high frequency of progenitors in the young pediatric samples, an age corresponding to the time of peak myelination, allowed us to identify these distinct stages of OL differentiation and maturation, each with its own unique transcriptional profile linked to their functional properties.

The use of the surgical tissue permits analysis of whole cells, including cytoplasmic RNA, of sufficient viability to be suitable for cell culture, in contrast to sequencing isolated nuclei, as has been previously performed on postmortem specimens, including from MS lesions (Jakel et al., 2019). The profile of cytosolic mRNA is distinct from that of nuclear mRNA (Chen, 2009). Therefore, compared to snRNA-seq studies, the transcriptional profiles of OL-lineage cells characterized here are more comparable to cells in vivo, since we were able to read transcripts from the whole cell. Although the resected tissue was obtained at sites distinct from the expected pathology and was normal appearing, we cannot be certain that there were no generalized transcriptomic alterations from the pathology for which the subject required surgery. Nonetheless, work by Gosselin et al. (2017) using similar pediatric surgical tissue indicated that derived microglia profiles largely reflected the physiologic state of the cells.



We note that employing the cell isolation procedure used here, OL-lineage cells constitute the majority of the cells isolated, followed by microglia and a few contaminating lymphocytes and astrocytes, in contrast to what is described in the autopsy based snRNA-seq results reported by Lake et al. (2017) and Jakel et al. (2019). Single cell nuclei staining data to date underrepresent the expected frequency of OL-lineage cells, especially from white matter samples. The observed paucity of neurons in our whole cell preparations could be explained in part because the samples were composed principally of white matter. We attribute the low number of astrocytes to the cell isolation procedure, particularly the percoll gradient step (Esmonde-White et al., 2019). Therefore, the cell isolation protocols and tissue dissociation methods appear to be a key determining factor of the frequency each cell type in the overall cell yield and is therefore a major source of heterogeneity across studies. Such discrepancies are apparent in our own experience when using surgical versus rapid autopsy materials (Wheeler et al., 2019). Other sources of variation in results across studies within the same species likely reflect samples being derived from distinct brain regions, different sequencing methodology, and/or the use of distinct bioinformatic analysis parameters.

The current analysis advances ongoing attempts to characterize populations of OLs at distinct stages of maturity and offers novel genetic targets for research studying demyelinating diseases. Our results correspond well with those described in the murine scRNA-seq study conducted by Artegiani et al. (2017), as we can recapitulate the key stage-specific identities of OL-lineage cells from healthy mouse tissue. The corresponding clusters in terms of maturity level display the highest percentage of overlapping genes, as would be expected (Supporting Information Figure S8).

The transcriptomic profile of our I-OPC subpopulation, which were the only progenitor type identified in our adult samples, overlaps considerably with the signature of the OPC cluster from Jakel et al. (2019), with key top genes including *SOX6*, *VCAN*, *MEGF11*, *HIF3A*, and *PTPRZ1*. However, our current MOL data does not resolve into their multiple described subclusters, instead displaying limited heterogeneity. We will continue to interrogate this finding using different bioinformatic techniques, but we elected to focus first on characterizing the progenitor populations here.

Additionally, although most often associated with myelinating Schwann cells in the peripheral nervous system, we detected expression of *PMP22* in MOL cells, consistent with reports of *PMP22* expression in the mature CNS (Ohsawa, Murakami, Miyazaki, Shirabe, & Sunada, 2006) and CNS pathology reported in some cases of Charcot Marie Tooth peripheral neuropathy due to *PMP22* gene duplication (Chanson et al., 2013).

Our gene ontology analysis, gene regulatory network analysis, and protein-protein interaction network analysis have provided insight into the potential functional significance of these cell subpopulations. We were particularly interested in I-OPCs given they are most highly represented at time of peak myelination and I-OPCs appear to be the only OL progenitor population that is present in adulthood. The most salient GO terms associated with this population were

related to the cell surface and ECM, which is composed of proteoglycans such as chondroitin and heparin sulfate proteoglycans, and hyaluronan, as well as collagens, laminins, fibronectin, and tenascins (Gundelfinger, Frischknecht, Choquet, & Heine, 2010). Cells interact with their local environment through the presentation of plasma membrane proteins and secretion of specific ECM components, and the ECM reciprocally modulates OL-lineage development through its mechanical-structural properties and extensive chemical signaling network (Colognato & Tzvetanova, 2011; Segel et al., 2019). Interestingly, multiple chondroitin sulfate proteoglycans, including *CSPG4*, and *VCAN*, were expressed more highly in the pediatric I-OPCs compared to the adult I-OPCs. In fact, it has been suggested that the scarcity of the ECM (Colognato & Tzvetanova, 2011) or the increase in ECM stiffness (Segel et al., 2019) associated with OL in the adult brain may be a contributing factor to its relatively poor capacity for remyelination. Gene products for secreted proteins that interact with and modify the functional properties of ECM were upregulated in I-OPCs, including, the chemotropic guidance cues *netrin-1* (*NTN1*), *semaphorins 5A and 5B* (*SEMA5A*, *SEMA5B*), and *SLIT1*, as well as key receptor and downstream signaling components linked to these factors, including *DSCAM*, *EPHB1*, *TRIO*, *CRMP1* and *FYN* (Brose & Tessier-Lavigne, 2000; DeGeer et al., 2015; Fiore & Puschel, 2003; Henderson & Dalva, 2018; Lai Wing Sun, Correia, & Kennedy, 2011; Norris, Sundararajan, Morgan, Roberts, & Lundquist, 2014; Rajasekharan et al., 2009). Genes encoding proteins that influence ECM remodeling were also upregulated, including *Tissue Inhibitor of Metalloproteinases 1* (*TIMP1*; Grunwald, Schoeps, & Kruger, 2019) and *SPARC-like protein 1* (*SPARCL1*; Jones & Bouvier, 2014). Together, these findings highlight specific cell surface and ECM genes as being among the most upregulated during peak myelinogenesis, supporting the conclusion that dynamic and active ECM remodeling is a key regulator of myelination across development. We have cross-referenced this data with rodent scRNA-seq data from healthy adult mouse brain tissue (Artegiani et al., 2017), and found that indeed their OPC population uniquely expressed ECM-related molecules such as *Cspg4*, *Fyn*, *Cspg5*, *Cntn1*, *Dscam*, *Sema5a*, *Trio* at the exclusion of MOLs, consistent with our findings. This was also the case in other datasets of adult human control brain (Jakel et al., 2019).

Additional upregulated local networks identified in I-OPCs included genes encoding cell-cell adhesion proteins, including *neuro-ligins* and *neurexins* (*NLGN4X*, *NRXN1*) and their interacting partner the *leucine-rich repeat transmembrane protein LRRTM1* (Reissner, Runkel, & Missler, 2013). Further, we detected upregulation of local networks associated with *leukotriene* signaling, implicated in OL survival (Ou et al., 2016), including the receptor *GPR17*, and *glutamate* signaling, including *metabotropic receptor GRM5*, and *AMPA type glutamate receptor subunits*, *GRIA2* and *GRIA3*, implicated in OPC maturation and functional diversification during development (Deng, Wang, Rosenberg, Volpe, & Jensen, 2004; Luyt, Varadi, Durant, & Molnar, 2006; Spitzer et al., 2019).

Other GO terms identified in I-OPCs highlighted cellular lipid metabolism, including *cholesterol transport*. Cholesterol is required for the formation of lipid rafts (Lingwood & Simons, 2010), specialized

plasma membrane microdomains that function as sites that focus transmembrane signal transduction and coordinate processes necessary for the initiation of myelination, such as cytoskeletal reorganization and recruitment of myelin-specific proteins (e.g., MBP and PLP1; Simons, Kramer, Thiele, Stoffel, & Trotter, 2000). The late myelin genes PLP1 and MBP, expressed in mature myelinating cells, were also upregulated in I-OPCs versus e-OPCs, consistent with their progression toward terminal differentiation and initial recruitment to early stages of myelin formation.

Overall, the coincident regulation of genes related to ECM composition, cholesterol metabolism and transport, and cell-cell adhesion in I-OPCs highlights the assembly of a cellular environment poised to commence myelination. Many of these processes are related through the activity of the tyrosine kinase FYN (Mathews et al., 2014), a key gene we find significantly upregulated in I-OPCs compared to e-OPCs and MOLs, which plays a central role in triggering OPC differentiation and promoting CNS myelination (Peckham et al., 2016; Rajasekharan et al., 2009; Sperber et al., 2001). Notably, the relatively high expression of FYN in the pediatric I-OPCs compared to the adult I-OPCs is consistent with previous studies reporting highest FYN expression during peak myelination (Kramer, Klein, Koch, Boytinch, & Trotter, 1999). The relative upregulation of MBP and CNP expression in pediatric I-OPCs compared to adult I-OPCs suggests that these cells are undergoing active differentiation. The presence of I-OPCs in adult cerebral cortex was validated in situ using the RNAScope approach, and the transcripts of both TNR and VCAN genes were found to be expressed with high specificity by these OL progenitors.

Gene regulatory network analysis indicated that each subpopulation has its own TF expression profile. Our centrality analysis showed that SOX2, upregulated in e-OPCs and I-OPCs compared to MOLs, was the most highly connected TF in all three subpopulations. This appears consistent with its known role in maintaining stemness of multipotent progenitor cells (Liu et al., 2013). In MOLs, SOX2 expression is markedly downregulated, as are many of the genes within its regulatory network. Given that SOX2 expression is necessary for proper remyelination in the adult brain (Zhang et al., 2018), the network of genes proximally regulated by SOX2 would be informative to study in the context of remyelination failure.

We acknowledge that RNA transcripts do not always reflect protein levels and recognize the key role of additional regulatory mechanisms for regulating protein expression, localization, and function. However, we can cite one related observation based on our previous work in which proteomic findings are in line with our current RNA findings. We observed that the myelin regulatory transcription factor TCF7L2 was predominantly detectable from full gestation to age 4 in humans by in situ immunohistochemistry (Lürbke et al., 2013). The TCF7L2 RNA transcript is most highly expressed increased in I-OPCs, whose presence in pediatric tissue is 22.5 times higher than in the adult tissue (17.37% pediatric: 0.77% adult, Figure 3b).

Overall, our work provides a valuable resource for the development of new stage specific markers of the OL-lineage, as well as potential targets for therapeutic interventions for demyelinating diseases. Going forward, further studies based on these findings will

investigate and identify novel contributions of these gene products to OL-lineage maturation and function.

In summary, our analysis of human brain tissue across a wide spectrum of ages, including the time of peak myelination, using a whole live cell scRNA-seq approach provides insight into the identity of subpopulations of OL-lineage cells that are distinct with respect to maturity and functional properties. This unbiased approach has identified novel genes whose role in the remyelination process remains to be further defined.

## ACKNOWLEDGMENTS

We thank Manon Blain for her technical assistance. This study was supported by a grant (BRAVEin MS) from the International Progressive MS Alliance (J.P.A.) and by a Genome Canada Genomic Technology Platform Grant and Compute Canada Resource Allocation Project wst-164 (IR).

## DATA AVAILABILITY STATEMENT

The differential expression data that support the findings of this study are available in the Supporting Information. All of the raw data for this study will be forthcoming.

## ORCID

Kelly Perlman  <https://orcid.org/0000-0002-2716-0712>

Qiao-Ling Cui  <https://orcid.org/0000-0002-2074-9655>

Luke Healy  <https://orcid.org/0000-0001-9496-2216>

Timothy E. Kennedy  <https://orcid.org/0000-0003-4454-5080>

## REFERENCES

- Artegiani, B., Lyubimova, A., Muraro, M., van Es, J. H., van Oudenaarden, A., & Clevers, H. (2017). A single-cell RNA sequencing study reveals cellular and molecular dynamics of the hippocampal neurogenic niche. *Cell Reports*, 21, 3271–3284.
- Baldassarro, V. A., Krężel, W., Fernández, M., Schuhbaur, B., Giardino, L., & Calzà, L. (2019). The role of nuclear receptors in the differentiation of oligodendrocyte precursor cells derived from fetal and adult neural stem cells. *Stem Cell Research*, 37, 101443.
- Blakemore, W. F., & Franklin, R. J. (2008). Remyelination in experimental models of toxin-induced demyelination. *Current Topics in Microbiology and Immunology*, 318, 193–212.
- Blondel, V. D., Guillaume, J.-L., Lambiotte, R., & Lefebvre, E. (2008). Fast unfolding of communities in large networks. *Journal of Statistical Mechanics: Theory and Experiment*, 2008, P10008.
- Brose, K., & Tessier-Lavigne, M. (2000). Slit proteins: Key regulators of axon guidance, axonal branching, and cell migration. *Current Opinion in Neurobiology*, 10, 95–102.
- Chanson, J. B., Echaniz-Laguna, A., Blanc, F., Lacour, A., Ballonzoli, L., Kremer, S., ... de Seze, J. (2013). Central nervous system abnormalities in patients with PMP22 gene mutations: A prospective study. *Journal of Neurology, Neurosurgery, and Psychiatry*, 84, 392–397.
- Chen, L. (2009). A global comparison between nuclear and cytosolic transcriptomes reveals differential compartmentalization of alternative transcript isoforms. *Nucleic Acids Research*, 38, 1086–1097.
- Colognato, H., & Tzvetanova, I. D. (2011). Glia unglued: How signals from the extracellular matrix regulate the development of myelinating glia. *Developmental Neurobiology*, 71, 924–955.
- Couturier, C. P., Ayyadury, S., Le, P. U., Monlong, J., Riva, G., Allache, R., ... Petrecca, K. (2018). Single-cell RNA-seq reveals that glioblastoma recapitulates normal brain development. *bioRxiv*, 449439.



- Cui, Q.-L., Khan, D., Rone, M., Rao, T. S. V., Johnson, R. M., Lin, Y. H., ... Antel, J. P. (2017). Sublethal oligodendrocyte injury: A reversible condition in multiple sclerosis? *Annals of Neurology*, 81, 811–824.
- DeGeer, J., Kaplan, A., Mattar, P., Morabito, M., Stochaj, U., Kennedy, T. E., ... Lamarche-Vane, N. (2015). Hsc70 chaperone activity underlies Trio GEF function in axon growth and guidance induced by netrin-1. *The Journal of Cell Biology*, 210, 817–832.
- Deng, W., Wang, H., Rosenberg, P. A., Volpe, J. J., & Jensen, F. E. (2004). Role of metabotropic glutamate receptors in oligodendrocyte excitotoxicity and oxidative stress. *Proceedings of the National Academy of Sciences of the United States of America*, 101, 7751–7756.
- Esmonde-White, C., Yaquib, M., Bilodeau, P.-A., Ling Cui, Q., Pernin, F., Larochelle, C., ... Antel, J. P. (2019). Distinct function-related molecular profile of adult human A2B5-positive pre-oligodendrocytes versus mature oligodendrocytes. *Journal of Neuropathology & Experimental Neurology*, 78, 468–479.
- Fernandez-Castaneda, A., & Gaultier, A. (2016). Adult oligodendrocyte progenitor cells—Multifaceted regulators of the CNS in health and disease. *Brain, Behavior, and Immunity*, 57, 1–7.
- Fiore, R., & Puschel, A. W. (2003). The function of semaphorins during nervous system development. *Frontiers in Bioscience*, 8, s484–s499.
- Gosselin, D., Skola, D., Coufal, N. G., Holtman, I. R., Schlachetzki, J. C. M., Sajti, E., ... Glass, C. K. (2017). An environment-dependent transcriptional network specifies human microglia identity. *Science*, 356(6344), eaal3222.
- Grunwald, B., Schoeps, B., & Kruger, A. (2019). Recognizing the molecular multifunctionality and interactome of TIMP-1. *Trends in Cell Biology*, 29, 6–19.
- Gundelfinger, E. D., Frischknecht, R., Choquet, D., & Heine, M. (2010). Converting juvenile into adult plasticity: A role for the brain's extracellular matrix. *The European Journal of Neuroscience*, 31, 2156–2165.
- Haghverdi, L., Büttner, M., Wolf, F. A., Büttner, F., & Theis, F. J. (2016). Diffusion pseudotime robustly reconstructs lineage branching. *Nature Methods*, 13, 845–848.
- Henderson, N. T., & Dalva, M. B. (2018). EphBs and ephrin-Bs: Trans-synaptic organizers of synapse development and function. *Molecular and Cellular Neurosciences*, 91, 108–121.
- Ilicic, T., Kim, J. K., Kolodziejczyk, A. A., Bagger, F. O., McCarthy, D. J., Marioni, J. C., & Teichmann, S. A. (2016). Classification of low quality cells from single-cell RNA-seq data. *Genome Biology*, 17, 29.
- Jakel, S., Agirre, E., Mendanha Falcao, A., van Bruggen, D., Lee, K. W., Knuesel, I., ... Castelo-Branco, G. (2019). Altered human oligodendrocyte heterogeneity in multiple sclerosis. *Nature*, 566, 543–547.
- Jones, E. V., & Bouvier, D. S. (2014). Astrocyte-secreted matricellular proteins in CNS remodelling during development and disease. *Neural Plasticity*, 2014, 321209.
- Kramer, E. M., Klein, C., Koch, T., Boytinch, M., & Trotter, J. (1999). Compartmentation of Fyn kinase with glycosylphosphatidylinositol-anchored molecules in oligodendrocytes facilitates kinase activation during myelination. *The Journal of Biological Chemistry*, 274, 29042–29049.
- Lachmann, A., Xu, H., Krishnan, J., Berger, S. I., Mazloom, A. R., & Ma'ayan, A. (2010). ChEA: Transcription factor regulation inferred from integrating genome-wide ChIP-X experiments. *Bioinformatics*, 26, 2438–2444.
- Lai Wing Sun, K., Correia, J. P., & Kennedy, T. E. (2011). Netrins: Versatile extracellular cues with diverse functions. *Development*, 138, 2153–2169.
- Lake, B. B., Chen, S., Sos, B. C., Fan, J., Kaeser, G. E., Yung, Y. C., ... Zhang, K. (2017). Integrative single-cell analysis of transcriptional and epigenetic states in the human adult brain. *Nature Biotechnology*, 36, 70.
- Lambert, S. A., Jolma, A., Campitelli, L. F., Das, P. K., Yin, Y., Albu, M., ... Weirauch, M. T. (2018). The human transcription factors. *Cell*, 172, 650–665.
- Lingwood, D., & Simons, K. (2010). Lipid rafts as a membrane-organizing principle. *Science*, 327, 46–50.
- Liu, K., Lin, B., Zhao, M., Yang, X., Chen, M., Gao, A., ... Lan, X. (2013). The multiple roles for Sox2 in stem cell maintenance and tumorigenesis. *Cellular Signalling*, 25, 1264–1271.
- Lürbke, A., Hagemeyer, K., Cui, Q.-L., Metz, I., Brück, W., Antel, J., & Kuhlmann, T. (2013). Limited TCF7L2 expression in MS lesions. *PLoS One*, 8, e72822.
- Luyt, K., Varadi, A., Durant, C. F., & Molnar, E. (2006). Oligodendroglial metabotropic glutamate receptors are developmentally regulated and involved in the prevention of apoptosis. *Journal of Neurochemistry*, 99, 641–656.
- Marques, S., Zeisel, A., Codeluppi, S., van Bruggen, D., Mendanha Falcao, A., Xiao, L., ... Castelo-Branco, G. (2016). Oligodendrocyte heterogeneity in the mouse juvenile and adult central nervous system. *Science*, 352, 1326–1329.
- Mathews, E. S., Mawdsley, D. J., Walker, M., Hines, J. H., Pozzoli, M., & Appel, B. (2014). Mutation of 3-hydroxy-3-methylglutaryl CoA synthase I reveals requirements for isoprenoid and cholesterol synthesis in oligodendrocyte migration arrest, axon wrapping, and myelin gene expression. *The Journal of Neuroscience—The Official Journal of the Society for Neuroscience*, 34, 3402–3412.
- Mathys, H., Davila-Velderrain, J., Peng, Z., Gao, F., Mohammadi, S., Young, J. Z., ... Tsai, L. H. (2019). Single-cell transcriptomic analysis of Alzheimer's disease. *Nature*, 570, 332–337.
- Miller, R. H. (2002). Regulation of oligodendrocyte development in the vertebrate CNS. *Progress in Neurobiology*, 67, 451–467.
- Miron, V. E., Kuhlmann, T., & Antel, J. P. (2011). Cells of the oligodendroglial lineage, myelination, and remyelination. *Biochimica et Biophysica Acta (BBA)—Molecular Basis of Disease*, 1812, 184–193.
- Norris, A. D., Sundararajan, L., Morgan, D. E., Roberts, Z. J., & Lundquist, E. A. (2014). The UNC-6/Netrin receptors UNC-40/DCC and UNC-5 inhibit growth cone filopodial protrusion via UNC-73/Trio, Rac-like GTPases and UNC-33/CRMP. *Development*, 141, 4395–4405.
- Ohsawa, Y., Murakami, T., Miyazaki, Y., Shirabe, T., & Sunada, Y. (2006). Peripheral myelin protein 22 is expressed in human central nervous system. *Journal of the Neurological Sciences*, 247, 11–15.
- Ou, Z., Sun, Y., Lin, L., You, N., Liu, X., Li, H., ... Chen, Y. (2016). Olig2-targeted G-protein-coupled receptor Gpr17 regulates oligodendrocyte survival in response to lysocleithin-induced demyelination. *The Journal of Neuroscience*, 36, 10560–10573.
- Peckham, H., Giuffrida, L., Wood, R., Gonsalves, D., Ferner, A., Kilpatrick, T. J., ... Xiao, J. (2016). Fyn is an intermediate kinase that BDNF utilizes to promote oligodendrocyte myelination. *Glia*, 64, 255–269.
- Rajasekharan, S., Baker, K. A., Horn, K. E., Jarjour, A. A., Antel, J. P., & Kennedy, T. E. (2009). Netrin 1 and Dcc regulate oligodendrocyte process branching and membrane extension via Fyn and RhoA. *Development*, 136, 415–426.
- Reissner, C., Runkel, F., & Missler, M. (2013). Neurexins. *Genome Biology*, 14, 213.
- Rueden, C. T., Schindelin, J., Hiner, M. C., DeZonia, B. E., Walter, A. E., Arena, E. T., & Eliceiri, K. W. (2017). ImageJ2: ImageJ for the next generation of scientific image data. *BMC Bioinformatics*, 18, 529.
- Schirmer, L., Velmeshev, D., Holmqvist, S., Kaufmann, M., Werneburg, S., Jung, D., ... Rowitch, D. H. (2019). Neuronal vulnerability and multilineage diversity in multiple sclerosis. *Nature*, 573, 75–82.
- Segel, M., Neumann, B., Hill, M. F. E., Weber, I. P., Viscomi, C., Zhao, C., ... Chalut, K. J. (2019). Niche stiffness underlies the ageing of central nervous system progenitor cells. *Nature*, 573, 130–134.
- Semple, B. D., Blomgren, K., Gimlin, K., Ferriero, D. M., & Noble-Haesslein, L. J. (2013). Brain development in rodents and humans: Identifying benchmarks of maturation and vulnerability to injury across species. *Progress in Neurobiology*, 106–107, 1–16.

- Simons, M., Kramer, E. M., Thiele, C., Stoffel, W., & Trotter, J. (2000). Assembly of myelin by association of proteolipid protein with cholesterol- and galactosylceramide-rich membrane domains. *The Journal of Cell Biology*, 151, 143–154.
- Sperber, B. R., Boyle-Walsh, E. A., Engleka, M. J., Gadue, P., Peterson, A. C., Stein, P. L., ... McMorris, F. A. (2001). A unique role for Fyn in CNS myelination. *The Journal of Neuroscience*, 21, 2039–2047.
- Spitzer, S. O., Sitnikov, S., Kamen, Y., Evans, K. A., Kronenberg-Versteeg, D., Dietmann, S., ... Karadottir, R. T. (2019). Oligodendrocyte progenitor cells become regionally diverse and heterogeneous with age. *Neuron*, 101, 459–471.e5.
- van Bruggen, D., Agirre, E., & Castelo-Branco, G. (2017). Single-cell transcriptomic analysis of oligodendrocyte lineage cells. *Current Opinion in Neurobiology*, 47, 168–175.
- Velmeshev, D., Schirmer, L., Jung, D., Haeussler, M., Perez, Y., Mayer, S., ... Kriegstein, A. R. (2019). Single-cell genomics identifies cell type—Specific molecular changes in autism. *Science*, 364, 685–689.
- Wheeler, M. A., Jaronen, M., Covacu, R., Zandee, S. E. J., Scalisi, G., Rothhammer, V., ... Quintana, F. J. (2019). Environmental control of astrocyte pathogenic activities in CNS inflammation. *Cell*, 176(3), 581–596.
- Zhang, S., Zhu, X., Gui, X., Croteau, C., Song, L., Xu, J., ... Guo, F. (2018). Sox2 is essential for oligodendroglial proliferation and differentiation during postnatal brain myelination and CNS remyelination. *The Journal of Neuroscience*, 38, 1802–1820.

#### SUPPORTING INFORMATION

Additional supporting information may be found online in the Supporting Information section at the end of this article.

**How to cite this article:** Perlman K, Couturier CP, Yaqubi M, et al. Developmental trajectory of oligodendrocyte progenitor cells in the human brain revealed by single cell RNA sequencing. *Glia*. 2020;1–13. <https://doi.org/10.1002/glia.23777>